Journal of Organometallic Chemistry 694 (2009) 3431–3437

Contents lists available at ScienceDirect

Journal of Organometallic Chemistry

journal homepage: www.elsevier.com/locate/jorganchem

Organotin(IV) 4-nitrophenylethanoates: Synthesis, structural characteristics and intercalative mode of interaction with DNA

Niaz Muhammad [a], Afzal Shah [a], Zia-ur-Rehman [a], Shaukat Shuja [a], Saqib Ali [a,*], Rumana Qureshi [a], Auke Meetsma [b], Muhammad Nawaz Tahir [c]

[a] Department of Chemistry, Quaid-i-Azam University, Islamabad 45320, Pakistan
[b] Crystal Structure Center, Chemical Physics, Zernike Institute for Advanced Materials, University of Groningen, Nijenborgh 4, NL-9747 AG Groningen, The Netherlands
[c] University of Sargodha, Department of Physics, Sargodha, Pakistan

ARTICLE INFO

Article history:
Received 9 April 2009
Received in revised form 18 June 2009
Accepted 23 June 2009
Available online 1 July 2009

Keywords:
Organotin
Crystal structures
Intercalation
Prostate cell lines (PC-3)

ABSTRACT

Four new organotin(IV) carboxylates, $[Bu_2SnL_2]$ **(1)**, $[Et_2SnL_2]$ **(2)**, $[Bu_3SnL]_n$ **(3)**, $[Me_3SnL]_n$ **(4)**, where L = 4-nitrophenylethanoates, were synthesized and characterized by elemental analysis, FT-IR and multinuclear NMR (^{1}H and ^{13}C). Spectroscopic results authenticated the coordination of ligand to the organotin moiety via COO group while X-ray single crystal analysis revealed bidentate chelating mode of coordination of ligand in complex **2** and a bridging behavior in complexes **3** and **4**. Cyclic voltammetric (CV) technique was used to evaluate the electrochemical, kinetic and thermodynamic parameters of complexes **1-4**, interacting with DNA. The linearity of the plots between the peak current (I) and the square root of the scan rate ($v^{1/2}$) indicated the electrochemical processes to be diffusion controlled. The diffusion coefficients of the free (D_f) and DNA bound forms (D_b), standard rate constants (ks) and charge transfer coefficients (α) were determined by the application of Randle–Sevcik, Nicholson and Kochi equations. Furthermore, the binding constants evaluated from voltammetric data revealed the following increasing order of binding strength: **2** < **1** < **4** < **3**. For **1** and **2**, the activity against prostate cancer cell lines (PC-3) was found consistent with the order obtained from voltammetric behavior.

1. Introduction

The booming application of metal complexes in the treatment of numerous human diseases is a vigorously expanding area in biomedical and inorganic chemistry [1,2]. The variation in coordination number, geometries, accessible redox states, thermodynamic and kinetic characteristics, and the intrinsic properties of the metal ion are some special characteristics of organometallic complexes that offer the medicinal chemists to employ different strategies for their exploitation. Their use in cancer chemotherapy is gaining mounting importance. Complexes of platinium(II) like cisplatin, oxalylplatin, nedaplatin and carboplatin have achieved clinical status as a result of intensive research focused on anticancer coordination compounds. However, in spite of having reasonable therapeutic index, the applications of metal complexes are limited by serious disadvantages like: (a) poor water solubility (b) toxicity and (c) the development of tolerance by the tumor. So the synthesis of non-platinum chemotherapeutics with positive, no or limited side effects is considered reasonable. Due to the potential antibacterial, antifungal and anticancer activity, organotins are the subject of intensive investigations [3–5]. However, in spite of such an importance the number of reports available on organotin(IV) carboxylates and their DNA binding properties are few. To bridge this gap we synthesized and structurally analyzed four novel organotin(IV) derivatives of 4-nitrophenylethanoate ligand. Furthermore, their DNA binding properties and anticancer activities against prostate cell lines (PC-3) were also evaluated. The objective of the current study is to provide useful insights in the understanding of drug-DNA interaction mechanism and drug design.

2. Experimental

All the organotin(IV) precursors were purchased from Aldrich and were used without further purification. All the solvents were dried according to reported procedures [6]. The melting points were recorded on an electrothermal melting point apparatus, model MP-D mitamura Riken Kogyo (Japan). Microanalysis was done using a Leco CHNS 932 apparatus. IR spectra were recorded with KBr pellets in the range from 4000–400 cm^{-1} using a Bio-Rad Excaliber FT-IR, model FTS 300 MX spectrometer (USA). Multinuclear NMR (^{1}H, ^{13}C) spectra were recorded at room temperature in $CDCl_3$ and DMSO-d_6 on a Bruker Advance Digital 300 MHz NMR spectrometer (Switzerland). DNA was extracted from human blood by

* Corresponding author. Tel.: +92 (051)90642130; fax: +92 (051)90642241.
E-mail address: drsa54@yahoo.com (S. Ali).

0022-328X/$ - see front matter © 2009 Elsevier B.V. All rights reserved.
doi:10.1016/j.jorganchem.2009.06.036

Falcon method [7]. The purity of DNA was checked from the ratio of absorbance at 260 and 280 nm (A_{260}/A_{280} = 1.85). The concentration of the stock solution of DNA (2.5 mM in nucleotide phosphate, NP) was determined by monitoring the absorbance at 260 nm, using the molar extinction coefficient (ε) of 6600 M^{-1} cm^{-1}. Electrochemical grade tetrabutylammonium fluoroborate (TBAFB) purchased from Fluka was used as supporting electrolyte. Dimethylsulphoxide (DMSO) with 99.5% purity was obtained from Riedal-de-Haën. Nitrogen saturated solutions were obtained by bubbling high purity N_2 for at least 10 min in the solution and keeping the environment of the pure gas over the solution during the voltammetric experiments. Electrochemical experiments were carried out using an Autolab PGSTAT 302 running with GPES (General-Purpose Electrochemical System) version 4.9, software (Eco-Chemie, Utrecht, The Netherlands). Voltammograms were recorded at room temperature using a three-electrode system. The working electrode was a glassy carbon electrode of 0.071 cm^2 area; saturated calomel electrode (SCE) was used as a reference electrode and a platinum wire as counter electrode. Prior to every electrochemical assay, the glassy carbon working electrode was polished with 0.25 μm diamond paste on a nylon buffing pad, followed by washing with water. All the experiments were carried out at room temperature (ca. 25 ± 1 °C).

2.1. Synthesis

2.1.1. Synthesis of Na-salt of 4-nitrophenylethanoic acid

The sodium salt of ligand, R′COONa, was prepared by dropwise addition of an equimolar amount of sodium hydrogen carbonate dissolved in distilled water to a methanolic solution of ligand acid (R′COONa). The solution was stirred for 2 h at room temperature and was evaporated under reduced pressure to give a white solid which was vacuum dried.

2.1.2. Dibutyltin(IV) bis(4-nitrophenylethanoate) (**1**)

The sodium salt R′COONa (1.02 g, 5 mmol), was refluxed for 10 h with dibutyltin(IV) dichloride (0.76 g, 2.5 mmol) in dry toluene contained in a 250 mL two neck round bottom flask. A turbid solution obtained, was left overnight at room temperature. The precipitated sodium chloride was filtered off and the filtrate was rotary evaporated. The resultant solid mass was recrystallized from chloroform and *n*-hexane (4:1) mixture. (Yield: 1.14 g, 77%). M.p. 89–92 °C. Anal. Calc. for $C_{24}H_{30}O_8N_2Sn$: C, 48.59; H, 5.10; N, 4.72. Found: C, 48.54; H, 5.07; N, 4.66%. IR (cm^{-1}): 1518 $\nu(OCO)_{asym}$, 1396 $\nu(OCO)_{sym}$, 511 ν(Sn–C), 468 ν(Sn–O). ^{1}H NMR ($CDCl_3$ and <DMSO>, ppm): 3.80 **<3.72>** (s, H_2, 4H); 7.50 <7.53> (d $H_{4,4'}$, 4H); 8.21 <8.17> (d, $H_{5,5'}$, 4H); 1.66-1.28 <1.33–1.108> (m, $H_{\alpha,\beta,\gamma}$, 12H); 0.83 <0.73> (t, H_δ, 6H). ^{13}C NMR ($CDCl_3$ and <DMSO-d_6>, ppm), ^nJ[(^{119}Sn, ^{13}C), Hz]: 180.3 <177.6> (C-1), 40.9 <41.6> (C-2), 141.7 <144.6> (C-3), 130.2 <131.1> (C-4), 123.8 <123.8> (C-5), 147.2 <146.7> (C-6), 25.34 <30.0> {C-α, [545<815>]}, 26.5 <27.2> {C-β, [36<39>]}, 26.2 <26.1> {C-γ, [87<90>] 13.5 <17.1> (C-δ).

2.1.3. Diethyltin(IV) bis(4-nitrophenylethanoate) (**2**)

Compound **2** was prepared and was recrystallized in the same way as **1**. R′COONa (1.02 g, 5 mmol), diethyltin(IV) dichloride (0.62 g, 2.5 mmol) (Yield: 1.20 g, 89%). M.p. 121–122 °C. Anal. Calc. for $C_{20}H_{22}O_8N_2Sn$: C, 44.72; H, 4.13; N, 5.22. Found: C, 44.41; H, 4.07; N, 5.19%. IR (cm^{-1}): 1521 $\nu(OCO)_{asym}$, 1389 $\nu(OCO)_{sym}$, 505 ν(Sn–C), 476 ν(Sn–O). ^{1}H NMR ($CDCl_3$ and <DMSO-d_6>, ppm), ^2J[(^{119}Sn, ^{1}H), Hz]: 3.80 <3.71> (s, H_2, 4H), 7.49 <7.53> (d, $H_{4,4'}$, 4H), 8.20 <8.20> (d, $H_{5,5'}$, 4H), 1.64 <1.30> {q, H_α, 4H [75]}, 1.22 <1.05> (t, H_β, 6H). ^{13}C NMR ($CDCl_3$ and <DMSO>, ppm), ^nJ[(^{119}Sn, ^{13}C), Hz]: 179.9 <177.4> (C-1), 40.9 <46.1> (C-2), 141.9 <144.9> (C-3), 130.2 <131.1> (C-4), 123.8 <123.6> (C-5), 147.1 <146.5> (C-6), 17.8 <23.6> {C-α, [584, <904>]}, 8.8 <10.0> {C-β, [<48.3>].

2.1.4. Tributyltin(IV) 4-nitrophenyl ethanoate (**3**)

Compound **3** was prepared in the same way as **1**, using equimolar molar amounts, R′COONa (1.02 g, 5 mmol) and tributyltin(IV) chloride (1.63 g, 5 mmol). The product was recrystallized from chloroform and *n*-hexane (4:1) mixture (Yield: 1.98 g, 84%). M.p. 60 °C. Anal. Calc. for $C_{20}H_{33}O_4NSn$: C, 51.09; H, 7.07; N, 2.98. Found: C, 51.04; H, 7.04; N, 2.94%. IR (cm^{-1}): 1553 $\nu(OCO)_{asym}$, 1392 $\nu(OCO)_{sym}$, 584 ν(Sn–C), 451 ν(Sn–O). ^{1}H NMR ($CDCl_3$ and <DMSO-d_6>, ppm): 3.73 <3.56> (s, H_2, 2H), 7.47 <7.49> (d, $H_{4,4'}$, 2H), 8.18 <8.14> (d, $H_{5,5'}$, 2H), 1.69-1.24 <1.54-1.18> (m, $H_{\alpha,\beta,\gamma}$, 18H), 0.90 <0.82> (t, H_δ, 9H). ^{13}C NMR ($CDCl_3$ and <DMSO-d_6>, ppm), ^nJ[(^{119}Sn, ^{13}C), Hz] : 175.1 <173.6> (C-1), 42.1 <43.6> (C-2), 143.5 <146.2> (C-3), 130.2 <131.0> (C-4), 123.6 <123.4> (C-5), 146.8 <146.3> (C-6), 16.6 <19.3> {C-α, [354, <470>]}, 27.7 <28.1> {C-β, [19, <27>]}, 27.0 <26.9> {C-γ, [65 <75>]}, 13.6 <14.1> (C-δ).

2.1.5. Trimethyltin(IV) 4-nitrophenylethanoate (**4**)

Compound **4** was prepared in the same way as **1**, using equimolar molar amounts, R′COONa (1.02 g, 5 mmol) and trimethyltin(IV) chloride (1.00 g, 5 mmol). The product was recrystallized from chloroform and *n*-hexane (4:1) mixture (Yield: 1.28 g, 74%). M.p. 142–144 °C. Anal. Calc. for $C_{11}H_{15}O_4NSn$: C, 38.41; H, 4.40; N, 4.07. Found: C, 38.36; H, 4.33; N, 4.04%. IR (cm^{-1}): 1514 $\nu(OCO)_{asym}$, 1343 $\nu(OCO)_{sym}$, 554 ν(Sn–C); 472 ν(Sn–O). ^{1}H NMR ($CDCl_3$ and <DMSO-d_6>, ppm), ^2J[(^{119}Sn, ^{1}H), Hz]: 3.74 <3.55> (s, H_2, 2H), 7.47 <7.48> (d $H_{4,4'}$, 2H), 8.19 <8.14> (d $H_{5,5'}$, 2H), 0.57 <0.37> {s, H_α, 9H, [58 <70>]}. ^{13}C NMR ($CDCl_3$ and <DMSO-d_6>, ppm), ^nJ[(^{119}Sn, ^{13}C), Hz]: 175.3 <173.8> (C-1), 41.7 <43.2> (C-2), 143.2 <146.0> (C-3), 130.3 <131.0> (C-4), 123.6 <123.5> (C-5), 146.9 <146.3> (C-6), -2.3 <0.7> {C-α, [386 <527>]}.

2.2. X-ray crystallographic studies

A crystal fragment, cut to size to fit in the homogeneous part of the X-ray beam, was mounted on top of a glass fiber and aligned on a Bruker SMART APEX CCD diffractometer (Platform with full three-circle goniometer). The crystal was cooled to 100(1) K using the Bruker KRYOFLEX low-temperature device. Intensity measurements were performed using graphite monochromatized Mo-K $\bar{\alpha}$ radiation from a sealed ceramic diffraction tube (SIEMENS). Data integration and global cell refinement was performed with the program SAINT [8]. The program suite SAINTPLUS was used for space group determination (XPREP) [8]. The structure was solved by Patterson method; extension of the model was accomplished by direct method and applied to difference structure factors using the program DIRDIF [9]. All refinement calculations and graphics were performed with the program PLUTO and PLATON package.

3. Results and discussion

3.1. Synthesis of complexes **1–4**

Reaction of R_3SnCl/R_2SnCl_2 with NaL in 1:1/1:2 molar ratios, respectively lead to the formation of complexes according to Eqs. (1) and (2) (Scheme 1). The resulting complexes were obtained in good yield (74–89%). All the complexes were white solids, stable in air and were soluble in $CHCl_3$ and DMSO. The numbering scheme of ligand and alkyl groups attached to Sn is shown in scheme 1.

3.2. IR spectra

By comparing the IR spectra of the free ligand with complexes **1–4**, the most explicit feature is the absence of a band in the region 3114–2571 cm^{-1}, which was due to –OH stretching vibration in the free ligand acid, thus signifying metal–ligand bond formation

$R_2SnCl_2 + 2NaL \longrightarrow R_2SnL_2 + 2NaCl$ (1)

R = n-Butyl (**1**), Ethyl (**2**)

$R_3SnCl + NaL \longrightarrow R_3SnL + NaCl$ (2)

R = n-Butyl (**3**), Methyl (**4**)

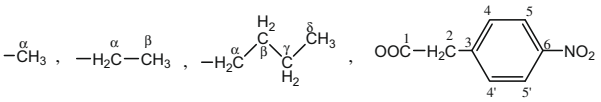

Scheme 1.

via this site. The absorption in the region 496–451 cm^{-1}, which was absent in the spectrum of the ligand acid, is assigned to the Sn–O stretching mode. All these values are consistent with literature values for a number of organotin–oxygen derivatives [10,11]. For organotin(IV) carboxylates, IR spectroscopy is helpful, pertaining to the mode of coordination of COO moiety [12]. The carboxylate group is acting as bidentate, if the Δv {ν_{asym}(COO)−ν-$_{sym}$(COO)} value, is smaller than 250 cm^{-1}. Values less than 150 cm^{-1} suggest a chelate structure, while difference between 150 cm^{-1} to 250 cm^{-1} put forward a bridged form. On the other hand, variation greater than 250 cm^{-1} would propose a monodentate coordination of the ligand. On the basis of Δv, the ligand surround the Sn atom in a chelated bidentate mode giving octahedral geometry to the complexes **1** and **2**, while the values observed for **3** and **4**, are compatible with a bridging bidentate bonding of the ligand in solid state. The structures proposed by the IR data matchwell with X-ray structures for complexes **2**, **3** and **4**.

3.3. NMR spectra

The assignment of the proton resonances were made by their peaks multiplicity, intensity pattern and comparison of the integration values of the protons with the expected composition. In the spectra of complexes **1–4**, the ligand furnished a sharp singlet in the aliphatic region due to CH_2 protons while aromatic protons gave two doublets in the expected region because of two non-equivalent sets of protons. The protons of the alkyl groups attached to Sn presented signals as expected [13,14]. The coordination around Sn atom was deduced from [^2J(^{119}Sn, ^{1}H)] coupling constant for compound **2** and **4**, the values observed were 75 and 58 Hz, respectively and consistent with CSnC angles of 124.96° and 111°, thus confirming five and four coordinated Sn atom in **2** and **4**, respectively, in solution [15]. ^{1}H NMR of complexes was also recorded in DMSO-d_6 and the data are given in brackets, < >. The [^2J (^{119}Sn, ^{1}H)] coupling constant in DMSO-d_6 indicated an increase in coordination number in **4**, thus confirm the coordination of DMSO with Sn atom.

The presence of the exact number of carbon resonances for ligand and alkyl groups as anticipated from the structures, in spectra of all complexes; validate the formation of complexes **1–4**. Furthermore, the signal of the carboxylic carbon of the ligand shifted downfield upon complexation. The ^1J [^{119}Sn, ^{13}C] coupling constant can be used to assess the coordination number of the Sn atom in organotin compounds. The coupling constants were calculated and found to be in the order of 545 Hz for dibutyltin **1** and 584 Hz for diethyltin **2** compounds which are consistent with the range reported for five coordinate Sn atom [13]. The calculated value of the ^1J [^{119}Sn, ^{13}C] coupling constant for **3** and **4** are 354 and 386 Hz, respectively describing the tetrahedral environment about the Sn atom in these compounds [16]. In order to check the effect of coordinating solvent, the ^{13}C NMR was also made in DMSO-d_6.

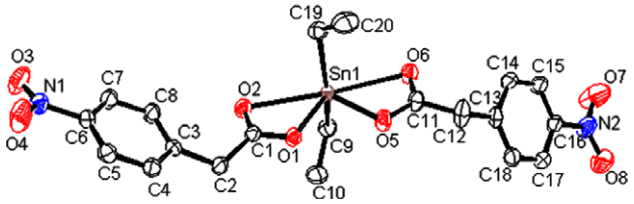

Fig. 1. ORTEP drawing of compound **2** with atomic numbering scheme.

The data indicated an increase in coordination sphere around Sn atom as can be seen from ^1J [^{119}Sn, ^{13}C] coupling constant values of complexes **1–4**.

3.4. Crystal structure of complex *2*, *3* and *4*

The structure of complex **2** is shown in Fig. 1. Crystal data and selected interatomic parameters are collected in Tables 1 and 2, respectively. The Sn atom in **2** is coordinated by two ethyl groups and two ligand molecules, with the later adopting different coordination modes. The two ligands are chelated to Sn in anisobidentate fashion, with one longer and one shorter Sn–O bond. The longer Sn–O distances are significantly less than the sum of the van der Waal's radii (3.68 Å) [17], and the coordination number of Sn is unambiguously assigned as six. The overall geometry at Sn is, however, highly distorted from the *trans* octahedral: the C–Sn–C angle is only 146.23 (15)°, so the Sn and four oxygen atoms of the two ligands are nearly coplanar but are highly distorted from square-planar geometry. The bond angles subtended at the Sn atom by the methylene carbons, O1 and O5 atoms vary from 101.67 (13)° to 104.23 (13)°, demonstrating that the Sn–C bonds are bent toward the longer Sn–O bonds. Thus, the coordination geometry about the Sn atom in compound **2** is best described as being distorted trapezoidal-bipyramidal. The geometry, bond lengths and angles of SnC_2O_4 core are comparable with literature values [5].

The molecular structures for complexes **3** and **4** are shown in Figs. 2 and 3, respectively. Pertinent crystallographic parameters, selected bond lengths and bond angles are given in Tables 1 and 3 (for compound **3**) and Table 4 (for compound **4**), respectively. The compounds **3** and **4** are zigzag chain polymers associating via bridging carboxylate ligands with *anti-syn* configuration. The Sn atoms in these polymeric structures exist in distorted trigonal bipyramidal environment with trigonal plane being defined by the three alkyl groups. The C–Sn–C angles are in the range, 115.95(17)–125.68(16)° and 117.37(8)–121.86(8)° for compounds **3** and **4**, respectively. The axial positions are occupied by two oxygen atoms of bridging carboxylate ligands with O–Sn–O angle is of the order of 177.38(10) and 170.30(4)° for tributyl- and trimethyltin(IV) derivatives, respectively. Thus, carboxylate ligand chelates the two symmetry related Sn atoms and gives rise to the unequal Sn–O bond distances. The inequality in the Sn–O bonds is reflected in the associated C–O bond lengths, the longer C–O bond is involved with shorter Sn–O interaction and vice versa. These bond lengths are in accord with the reported triorganotin(IV) carboxylates [18].

3.5. Cyclic voltammetry of complexes *1–4*

The cyclic voltammetric behavior of complexes **1–4** on bare glassy carbon electrode was studied in the absence and presence of DNA, in 10% aqueous DMSO at 25 °C. The voltammograms of all of the complexes showed a pair of redox waves with ΔE_p = 124–207 mV, indicating quasi-reversibility of their electrochemical processes. Typical CV behavior of **1**, with and without DNA is shown in Fig. 4. Due to the instability of Sn^{+3}, the voltam-

Table 1
Crystal data and structure refinement parameters for compound **2**, **3** and **4.**

Compound	**2**	**3**	**4**
Moiety formula	$C_{20}H_{22}N_2O_8Sn$	$C_{20}H_{33}NO_4Sn$	$C_{11}H_{15}NO_4Sn$
Formula weight	537.09	470.20	343.95
Crystal system	Triclinic	Tetragonal	Monoclinic
Space group	*P*-1	$P4_32_12$	$P2_1/c$
Unit cell dimensions			
a (Å)	9.6184(5)	9.6208(6)	10.6979(5)
b (Å)	10.7133(5)	–	10.0491(5)
c (Å)	11.2762(5)	49.564(6)	12.4860(6)
β (°)	98.992(2)	–	107.2835(7)
V (Å^3)	1085.23(9)	4587.6(7)	1281.69(11)
θ ranges for data collection (°)	1.85–28.73	2.45–26.37	2.65–28.28
Z	2	8	4
$\rho_{calc.}$ (g cm^{-3})	1.644	1.361	1.782
F(0 0 0)	540	1936	680
crystal size mm	0.30 × 0.22 × 0.15	0.23 × 0.19 × 0.15	0.32 × 0.26 × 0.14
Index ranges	h: −12 → 12; k: −14 → 14; l: −15 → 15	h: −11 → 12; k: −12 → 11; l: −61 → 59	h: −14 → 14; k: −12 → 13; l: −16 → 16
Total data	20328	36409	11327
Unique data (R_{int})	549 (0.0381)	4668 (0.0759)	3189 (0.0169)
Final *R* indices ($I>/4\sigma(I)$)	R_1 = 0.0375	R_1 = 0.0378	R_1 = 0.0191
	wR_2 = 0.1015	wR_2 = 0.0794	wR_2 = 0.0478

Table 2
Selected bond lengths (Å) and bond angles (°) of compound **2.**

Sn1–O1	2.116(2)	Sn1–C19	2.111(4)
Sn1–O2	2.606(3)	O1–C1	1.281(4)
Sn1–O5	2.110(2)	O2–C1	1.239(4)
Sn1–O6	2.629(3)	O5–C11	1.282(4)
Sn1–C9	2.111(3)	O6–C11	1.228(4)
C9–Sn1C19	146.23(15)	C19–Sn1–O6	89.93(12)
C9–Sn1–O1	102.77(12)	O1–Sn1-O2	54.01(10)
C9–Sn1––O2	85.63(13)	O1–Sn1–O5	81.40(9)
C9–Sn1–O5	101.67(13)	O1–Sn1–O6	134.83(10)
C9–Sn1–O6	88.37(12)	O2–Sn1–O5	135.17(10)
C19–Sn1–O1	102.19(12)	O2–Sn1–O6	170.51(9)
C19–Sn1–O2	90.98(13)	O5–Sn1–O6	53.43(10)
C19–Sn1–O5	104.23(13)		

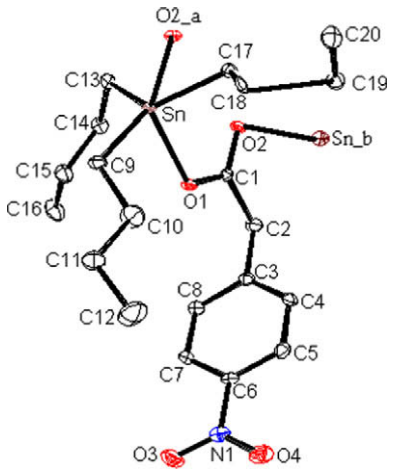

Fig. 2. ORTEP drawing of compound **3** with atomic numbering scheme.

metric response is attributed to the 2e redox process of Sn^{+2}/Sn^{+4} couple. In the absence of DNA, compound **1** registered a cathodic peak at −1.212 V and anodic peak at −1.014 V. The large peak to peak potential difference (ΔE_p) of 198 mV is suggestive of electrochemical reaction coupled with a chemical reaction. With the increase in concentration of DNA in a constant amount of compound **1,** the voltammetric response of the compound altered as is manifested by the sequential drop in peak current and gradual

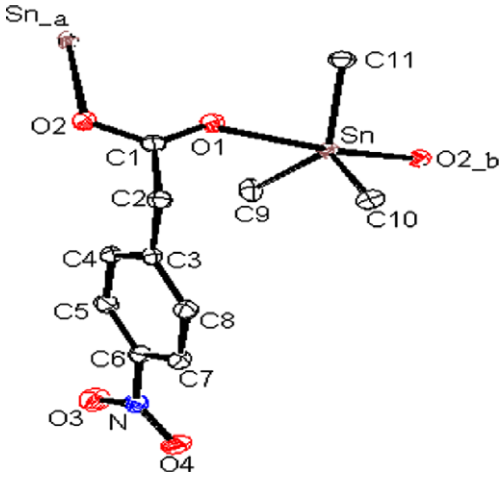

Fig. 3. ORTEP drawing of compound **4** with atomic numbering scheme.

peak potential shift in positive direction. The shift of peak potential to less negative values is suggestive of intercalation of **1** into DNA [19]. The observed decrease in peak current indicates the formation of large and slowly diffusing **1**-DNA adduct due to which the free drug concentration (which is mainly responsible for the conduction of the current) is lowered. The electrochemical parameters of complexes **1–4**, in the absence and presence of 60 μM DNA are listed in Table 5. The results reveal that the formal potential varies in the sequence: 1 > 3 > 4 > 2, suggesting more easy oxidation of 1 and 3, which can be due to the strong electron-donating ability of

Table 3
Selected bond lengths (Å) and bond angles (°) of complex **3**.

Sn–O1	2.189(3)	Sn–C13	2.152(5)
Sn–O2_a	2.377(3)	Sn–C17	2.147(4)
Sn–C9	2.146(4)	O1–C1	1.273(5)
O2–C1	1.245(5)		
O1–Sn–C9	89.95(13)	C9–Sn–O2_a	87.52(12)
O1–Sn–C13	96.38(14)	C13–Sn–C17	125.68(16)
O1–Sn–C17	96.28(14)	C13–Sn–O2_a	84.16(14)
O1–Sn–O2_a	177.38(10)	C17–Sn–O2_a	85.45(14)
C9–Sn–C13	116.65(17)	Sn–O1–C1	115.9(2)
C9–Sn–C17	115.95(17)		

Table 4
Selected bond lengths (Å) and bond angles (°) of compound **4.**

Sn–O1	2.5422(13)	Sn–C11	2.121(2)
Sn–O2_b	2.1717(12)	O1–C1	1.238(2)
Sn–C9	2.123(2)	O2–C1	1.285(2)
Sn–C10	2.1177(19)		
O1–Sn–O2_b	170.30(4)	O2_b–Sn–C10	100.71(6)
O1–Sn–C9	86.34(6)	O2_b–Sn–C11	89.85(7)
O1–Sn–C10	87.28(6)	C9–Sn–C10	117.37(8)
O1–Sn–C11	81.44(6)	C9–Sn–C11	121.86(8)
O2_b–Sn–C9	94.73(7)	C10–Sn–C11	118.49(8)

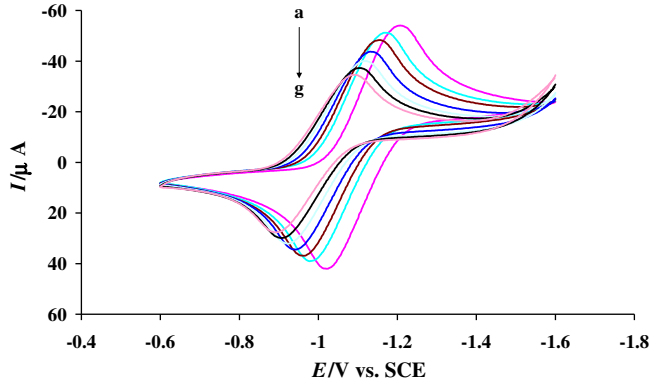

Fig. 4. CV behavior of 3 mM **1** at GC electrode in the absence (a) and presence of 10 (b), 20 (c), 30 (d), 40 (e), 50 (f) and 60 μM DNA (g) in 10 % aqueous DMSO with 0.1 M TBAFB as supporting electrolyte at 0.1 V/s scan rate.

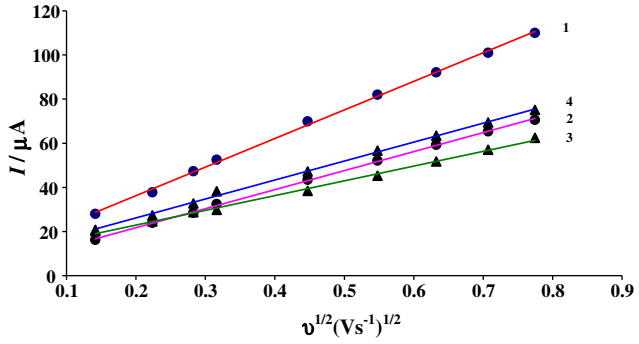

Fig. 5. Plots of I vs. $v^{1/2}$, for the determination of the diffusion coefficients of 3 mM **1**, **2**, **3** and **4.** Scan rates: 0.02, 0.05, 0.08, 0.1, 0.2, 0.3, 0.4, 0.5 and 0.6 Vs^{-1}.

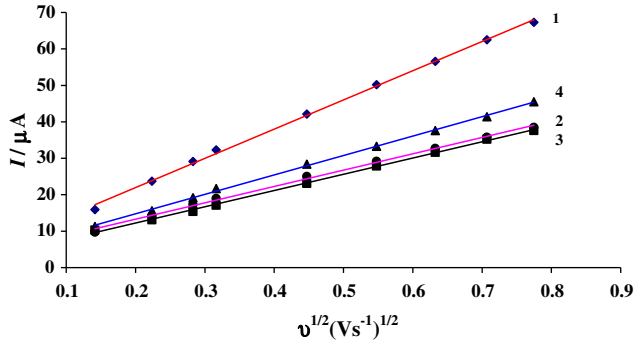

Fig. 6. Plots of I vs. $v^{1/2}$, for the determination of the diffusion coefficients of 3 mM **1**, **2**, **3** and **4**, in the presence of 60 μM DNA. Scan rates: 0.02, 0.05, 0.08, 0.1, 0.2, 0.3, 0.4, 0.5 and 0.6 Vs^{-1}.

butyl groups. The behavior is consistent with the generalization that electron-donating groups facilitate oxidation by shifting the formal potential (E^o) in more negative direction while electron-withdrawing groups make the oxidation difficult by shifting the E^o to less negative values. The shift of formal potentials of these complexes to less negative values by the addition of DNA could be correlated to their intercalation into the stacked base pairs pockets of DNA as suggested by the previous researchers [19]. The values of $\Delta E_p > 60 < 212$ and $I_{pc}/I_{pa} > 1$ shown in Table 5, reflect the redox processes of the free and DNA-bound complexes to be quasi-reversible.

The diffusion coefficients of the free and DNA-bound complexes were determined by the application of Randle–Sevcik expression [20,21]:

$$I = 2.69 \times 10^5 n^{3/2} A C_o D_o^{1/2} v^{1/2} \quad (1)$$

where, I is the peak current (A), A is the surface area of the electrode (cm^2), C_o is the bulk concentration (mol cm^{-3}) of the electroactive species, D_o is the diffusion coefficient (cm^2 s^{-1}) and ν is the scan rate (V s^{-1}).

The linearity of I vs $v^{1/2}$ plots (Figs. 5 and 6) demonstrates, that the main mass transport of these complexes (in the absence and presence of DNA) to the electrode surface is diffusion controlled. The values of the diffusion coefficient (D_f) listed in Table 6 vary in the order: **1** > **2** > **4** > **3**, indicating greater D_f of **1** and **2** than **4** and **3**, owing to higher coordination number which effectively blocks the central metal ion (Sn^{+4}), thereby decreasing the chances of its attachment with the solvent. In case of **3** and **4**, the lower coordination number allows the central metal ion to be interacted by the solvent, thereby minimizing their rates of diffusion. The greater D_f value of **1** as compared to **2** can be explained by the presence of more lyophobic butyl groups than ethyl groups. The lower D_f value of **3** than **4** is due to higher molecular weight, confirming

Table 5
CV data of compounds **1**–**4.**

Compound	CV data						
	E_{pa} (V)	E_{pc} (V)	ΔE_p (mV)	E° (V)	I_{pa}(μA)	I_{pc}(μA)	I_{pc}/I_{pa}
1	−1.014	−1.212	198	−1.113	41.91	53.99	1.29
1-DNA	−0.890	−1.097	207	−0.994	27.63	34.48	1.25
2	−1.019	−1.187	168	−1.103	21.75	38.81	1.78
2-DNA	−0.885	−1.063	178	−0.974	15.16	23.90	1.58
3	−1.043	−1.173	130	−1.108	21.14	28.71	1.36
3-DNA	−0.921	−1.063	153	−0.992	11.33	16.39	1.45
4	−1.044	−1.170	126	−1.107	24.04	32.38	1.35
4-DNA	−0.897	−1.046	149	−0.972	13.08	18.88	1.44

All potentials were measured versus SCE in 10% aqueous DMSO at 0.1 Vs^{-1}.
$\Delta E_p = (E_{pa} - E_{pc})$.
$E^{\circ} = (E_{pa} + E_{pc})/2$.

Table 6
Summary of kinetic and thermodynamic data of free and DNA bound forms of compounds **1**–**4**, as obtained from electrochemical measurements.

Compound	Kinetic data				Thermodynamic data	
	$D_f \times 10^7$ (cm^2/s)	$D_b \times 10^7$ (cm^2/s)	$k_s \times 10^4$ (cm/s)	α	$K \times 10^{-4}$ (M^{-1})	ΔG (kJmol^{-1})
1	6.54 (±0.19)	–	5.04(±0.20)	0.54(±0.02)	–	–
1-DNA	–	2.44(±0.11)	2.86(±0.14)	0.51(±0.01)	1.11(±0.04)	23.08(±0.93)
2	2.85(±0.09)	–	4.39(±0.17)	0.54(±0.02)	–	–
2-DNA	–	1.08(±0.05)	2.44(±0.15)	0.51(±0.01)	0.85(±0.03)	22.42(±0.89)
3	1.70(±0.07)	–	5.91(±0.26)	0.63(±0.03)	–	–
3-DNA	–	0.756(±0.04)	2.73(±0.17)	0.54(±0.02)	1.46(±0.05)	23.76(±1.19)
4	2.80(±0.08)	–	8.64(±0.35)	0.53(±0.02)	–	–
4-DNA	–	0.764(±0.04)	2.95(±0.16)	0.62(±0.03)	1.39(±0.07)	−23.64(±1.18

the idea that a heavy molecule diffuses slowly to the electrode surface.

The D_b values of the DNA bound complexes, summarized in Table 6, follow the same order as was observed for the D_f of the free complexes. The D_b values are lower than the D_f values because of the interaction of these complexes to the large and slowly moving DNA.

The values of standard rate constant (ks) of the electron transfer reaction of these complexes at the electrode surface were obtained from Nicholson equation [22]:

$$\psi = \frac{ks}{\left[\pi D_o \frac{nfv}{RT}\right]^{1/2}} \quad (2)$$

where ψ is a dimensionless parameter (depending upon peak separation, ΔE_p) and all other parameters have their usual significance.

An examination of Table 6 reflects that the values of ks are of the order of 10^{-4} cms^{-1}, offering another evidence for the quasi-reversibility of the redox processes with slow electron transfer kinetics. Table 6, further signifies lower ks values of complex–DNA adducts as compared to the free complexes due to their lower diffusion coefficients.

The values of charge transfer coefficient (α) were determined by the application of Kochi formula [23]:

$$\alpha = \left[\frac{(E_{1/2} - E_p^c)}{(E_p^a - E_p^c)}\right] \quad (3)$$

α with values of more than 0.5 for all the four complexes (with and without DNA) further established the quasi-reversibility of the electrochemical processes.

The gradual decay in peak current of the complexes by the addition of varying concentration of DNA, ranging from 20 to 60 μM, can be used to quantify the binding constant by using the following equation [24]:

$$log\,(1/[DNA]) = log\,K + log\,(I_{H-G}/(I_G - I_{H-G})) \quad (4)$$

where, K is the binding constant, I_G and I_{H-G} are the peak currents of the free guest (G) and the complex (H–G), respectively.

The binding constant, $K = 1.11 \times 10^4$ and 8.50×10^3 M^{-1}, for the interaction of **1** and **2** with DNA were obtained, respectively from the intercept of log (1/[DNA]) versus log ($I_{H-G}/(I_G - I_{H-G})$) plots (Fig. 7). The greater K of **1** than **2**, is presumably due to the additional hydrophobic interactions of the bulky butyl groups with the nucleotide bases as compared to ethyl groups [25]. The same attribution is assigned to the strong binding constant of **3** ($K = 1.46 \times 10^4$ M^{-1}) than **4** ($K = 1.39 \times 10^4$ M^{-1}). The results further verified that complexes **3** and **4** show stronger affinity for DNA than **1** and **2**. The greater K of these Sn complexes than those observed for similar DNA-intercalating Cr and Ru complexes; $[CrCl_2(dicnq)_2]^+$ and $[Ru((dicnq)_3]^{+2}$, with K reported as 1.20×10^3 and 9.70×10^3 M^{-1} [25–27], suggests their potential candidature as chemotherapeutic agents. The negative values of standard Gibbs free energy ($\Delta G = -RT \ln K$) indicate the spontaneity of the binding interaction of these complexes with DNA.

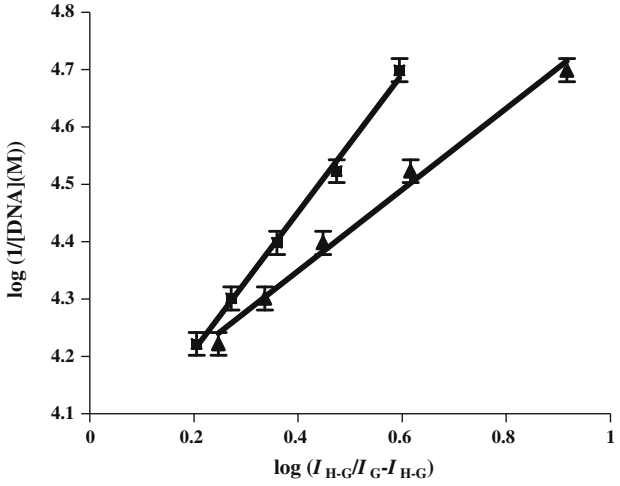

Fig. 7. Plots of log ($I_{H-G}/(I_G - I_{H-G})$) *vs.* log (1/[DNA]) used to calculate the binding constants of **2**-DNA (■) and **1**-DNA (▲) complexes.

Table 7
In vitro anticancer results (IC_{50}, μg/mL) of compounds **1** and **2**.

Compound no.	PC-3
1	2.53 ± 0.94
2	7.92 ± 0.65
[a]Doxorubicin	0.912

[a] Standard drug used.

3.6. Anticancer activity

The in vitro anticancer activity of compounds **1** and **2** against prostate cancer cells (PC-3) was evaluated according to the literature reported method [28]. The data (Table 7) indicate that the compound **1** is a potential anticancer agent as compared to **2**, and consistent with the trend observed in electrochemical study.

4. Conclusion

The outcome of the present study is that the di- and triorganotin(IV) 4-nitrophenylethanoates demonstrated different structural motifs in solution and solid states. Regarding the DNA-binding study, the most promising feature is the intercalative mode of interaction of these complexes with DNA with experimental proof from electrochemical study which according to our survey is a new contribution to organotin(IV) carboxylates. Apart from this, the diffusion coefficient of the compounds decrease with the increase in molecular weight but is not a sole factor because geometry also

plays a decisive role as evident from our results. The lower *k*s values of the DNA bound complexes as compared to free complexes indicated slower electron transfer kinetics. The charge transfer coefficient ($\alpha > 0.5$), ratio of peak currents ($I_{pc}/I_{pa} > 1$) and peak potential difference ($\Delta E_p > 60 < 212$) point to the quasi-reversibility of the redox processes. The binding constants and the Gibbs free energy varied in the sequence: **3** > **4** > **1** > **2**.

Acknowledgement

We thank the Higher Education Commission of Pakistan for financial support.

Appendix A. Supplementary material

CCDC 719410, 718881 and 718880 contain the supplementary crystallographic data for **2**, **3** and **4**, respectively. These data can be obtained free of charge from The Cambridge Crystallographic Data Centre via www.ccdc.cam.ac.uk/data_request/cif. Supplementary data associated with this article can be found, in the online version, at doi:10.1016/j.jorganchem.2009.06.036.

References

[1] P.B. Blower, Annu. Rep. Prog. Chem., Sect. A 97 (2001) 587–603.
[2] J.L. Sessler, S.R. Doctrow, J. McMurry, S.J. Lippard (Eds.), Medicinal Inorganic Chemistry, American Chemical Society, Washington, DC, 2005.
[3] T.S.B. Baul, S. Dutta, E. Rivarola, M. Scopelliti, S. Choudhuri, Appl. Organomet. Chem. 15 (2001) 947–953.
[4] N. Muhammad, Z. Rehman, S. Ali, A. Meetsma, F. Shaheen, Inorg. Chim. Acta 362 (2009) 2842–2848.
[5] A. Růžička, L. Dostál, R. Jambor, V. Buchta, J. Brus, Appl. Organomet. Chem. 16 (2002) 315–322.
[6] D.D. Perrin, W.L.F. Armengo, Purification of Laboratory Chemical, third ed., Pergamon Press, Berlin, Oxford, 2003.
[7] J. Sambrook, E.F. Fritsch, T. Maniatis, Molecular Cloning: A Laboratory Manual, second ed., Cold Spring Harbour Laboratory Press, New York, 1989.
[8] Bruker, SMART, SAINTPLUS and XPREP. Area Detector Control and Integration Software. Smart Apex Software Reference Manuals, Bruker Analytical X-ray Instruments, Inc., Wisconsin, USA, 2006.
[9] P.T. Beurskens, G. Beurskens, R. de Gelder, S. García-Granda, R.O. Gould, R. Israël, J.M.M. Smits, The DIRDIF-99 program system, Crystallography Laboratory, University of Nijmegen, The Netherlands, 1999.
[10] R.R. Holmes, C.G. Schmid, V. Chandrasekhar, R.O. Day, J.M. Homels, J. Am. Chem. Soc. 122 (2000) 5158–5168.
[11] G.K. Sandhu, R. Hundal, J. Organomet. Chem. 436 (1992) 287–298.
[12] G. Eng, X. Song, A. Zapata, A.C. de Dios, L. Casabianca, R.D. Pike, J. Organomet. Chem. 692 (2007) 1398–1404.
[13] Z. Rehman, M. Barsan, I. Wharf, N. Muhammad, S. Ali, A. Meetsma, I.S. Butler, Inorg. Chim. Acta 361 (2008) 3322–3326.
[14] S. Shahzadi, S. Ali, M.H. Bhatti, M. Fettouhi, M. Akhtar, J. Organomet. Chem. 691 (2006) 1797–1802.
[15] T.P. Lockhart, W.F. Manders, Inorg. Chem. 25 (1986) 892–895.
[16] M.K. Rauf, M.A. Saeed, J. Organomet. Chem. 693 (2008) 3043–3048.
[17] E.R.T. Tiekink, Trends Organomet. Chem. 1 (1994) 71–116.
[18] C.L. Ma, Q.F. Zhang, R.F. Zhang, L.L. Qiu, J. Organomet. Chem. 690 (2005) 3033–3043.
[19] A. Shah, A.M. Khan, R. Qureshi, F.L. Ansari, M.F. Nazar, S.S. Shah, Int. J. Mol. Sci. 9 (2008) 1424–1434.
[20] J.E.B. Randles, Trans Faraday Soc. 44 (1948) 327–338.
[21] A. Sevcik, Collect. Czech Chem. Commun. 13 (1948) 349–377.
[22] E. Niranjana, R.R. Naik, B.E.K. Swamy, Int. J. Electrochem. Sci. 3 (2008) 980–992.
[23] R.J. Klinger, J.K. Kochi, J. Phys. Chem. 85 (1981) 1731–1741.
[24] Q. Feng, N.Q. Li, Y.Y. Jiang, Anal. Chim. Acta 344 (1997) 97–104.
[25] Q. Lie, P. Yang, H. Wang, M. Guo, J. Inorg. Biochem. 64 (1996) 181–195.
[26] J. Rusanova, S. Decurtins, E. Rosanov, H.S. Evans, S. Delahaye, A. Hauser, J. Chem. Soc. Dalton Trans. (2002) 4318–4320.
[27] A. Ambroise, B.G. Maiya, Inorg. Chem. 39 (2000) 4264–4272.
[28] P. Skehan, R. Storeng, D. Scudiero, A. Monks, J. McMahon, D. Vistica, J.T. Warren, H. Bokesch, S. Kenney, M.R. Boyd, J. Natl, Cancer Inst. 82 (1990) 1107–1112.